COBEM 2023 27TH INTERNATIONAL CONGRESS OF MECHANICAL ENGINEERING

ABCM Brazilian Society of Mechanical Sciences and Engineering
27th ABCM International Congress of Mechanical Engineering
December 04-08, 2023, Florianópolis-SC, Brazil

COB-2023-1446
INVESTIGATING THE RELATIONSHIP BETWEEN MASS AND FLEXURAL RESISTANCE IN MATERIAL EXTRUSION ADDITIVE MANUFACTURING OF CARBONYL IRON COMPONENTS: A COMPARATIVE STUDY WITH METAL INJECTION MOLDING

Augusto Adami Vidal
Fernando Irto Zanetti
Federal University of Santa Catarina – Laboratório de Materiais - Department of Mechanical Engineering – Florianópolis/SC
augusto.a.v@labmat.ufsc.br
fernando.i.z@labmat.ufsc.br

Gustavo Alves Lau
Guilherme Breda Fatall
Arthur Garcia Lima Cruz
Aloisio Nelmo Klein
Rodrigo Perito Cardoso
Federal University of Santa Catarina – Laboratório de Materiais - Department of Mechanical Engineering – Florianópolis/SC
gustavo.lau@labmat.ufsc.br
guilherme.b.f@labmat.ufsc.br
arthur.l.c@labmat.ufsc.br
a.n.klein@labmat.ufsc.br
rodrigo.perito@ufsc.br

Abstract. *Material Extrusion Additive Manufacturing (MEX) is an outstanding technology that allows an efficient and cost-effective solution for multi-step fabrication of metallic components without tools or molds shape limitations. Nowadays, some mechanical parts, like gears and structural elements, are oversized due limitations of conventional manufacturing methods like machining and casting. This study aims to evaluate the capabilities and mechanical properties of MEX components, fabricated via a screw-based device, by conducting a flexural test analysis using three different filling densities to optimize mass and perform resistance analysis, aiming the primary objective of determining the relationship between flexural resistance and component mass. Samples were produced by traditional MIM process and MEX additive manufacturing, both with carbonyl iron-based feedstock applied in pellet form for the MIM process, and powder form for MEX fabrication. Once manufactured via MIM and MEX, samples undergo chemical debinding and sintering via a plasma-assisted method in the same batch. The specimens produced using MEX will feature the same infill parameter, namely a grid parameter with orthogonal lines, with different infill density, while others printing parameters are held constant. Results from the MEX components were compared with those fabricated via Metal Injection Molding (MIM). The samples were evaluated according to the ISO 178 standard, which involves a flexural test analysis widely utilized for assessing the mechanical behavior of polymeric and MIM specimens. Through this methodology, we determined the specific resistance of the samples by analyzing their resistance as a function of mass. The specific resistance was then compared to that of the MIM specimens, which serve as the benchmark for this study. In conclusion, it was possible to demonstrate the optimization of the resistance/mass relation in the MEX specimens.*

Keywords: *Material Extrusion Additive Manufacturing, Mechanical Properties, Mass Optimization, Powder Metallurgy, Plasma Sintering, Flexural Test.*

1. INTRODUCTION

Additive manufacturing (AM) is a flexible method to fabricate personalized products, offering low weight and tailored properties in mechanical, electrical and thermal aspects (Gonzalez-Gutierrez et al., 2010). In the past decade, material extrusion additive manufacturing (MEX) has gained popularity for metallic components due to its simplicity, safety, cost-effectiveness and minimal material waste compared to other metallic AM techniques (Suwanpreecha et al., 2023; Gonzalez-Gutierrez et al., 2021).

Currently, structural mechanical components often exhibit an reducible mass due to the limitation of creating a non-communicating cavity with the component surface using conventional manufacturing methods such as casting and machining (Beeley, 2001; Astakhov et al., 2010). On the other hand, AM, with its layer-by-layer manufacturing approach, enables the creation of specimens with internal cavities, offering a practical solution to reduce the mass of components (Gonzalez-Gutierrez et al., 2021; Gibson et al., 2010). In light of these considerations, the present study aims to investigate the relationship between mass and flexural resistance of MEX components manufactured using a screw-based device. MIM specimen's response to flexural stress served as a point of reference for comparative analysis. This investigation focuses on the production of carbonyl iron specimens that do not possess 100% geometrical density, which represents a significant advantage of AM (Gonzalez-Gutierrez et al., 2021). The study involves the fabrication and characterization of carbonyl iron parts with varying infill grades through the MEX, chemical debinding and plasma sintering techniques. The same methodology of debinding and sintering was employed for MIM specimens. The feedstock for both processes, MEX and MIM, consists of a MIM feedstock pellets made of polypropylene (PP), ethylene-vinyl acetate (EVA) and paraffin as the matrix of the granules with dispersed carbonyl iron powder. It was processed into a powder to be applied in the MEX machine. Printing parameters were maintained constants for the four different printed samples, that is: 25%, 50%, 75%, and 90% infill percentages. MIM samples were produced using an Arburg 320s injection molding machine. Then, chemical debinding was runned through a Lömi solvent debinding system. Finally, sintering was conducted at a cold plasma reactor.

For engineering applications subject to bending stresses, design considerations revolve around the moment of inertia of the area. The moment of inertia is computed by integrating the area with respect to its distance from the axis of rotation. In this context, the farther an area is from the axis of rotation, the more significant its contribution becomes. This concept finds broad application, particularly in the use of trusses, which are structures primarily engineered to withstand bending forces while minimizing mass. This is one distinctive feature of the Material Extrusion (MEX) additive manufacturing technique, the fabrication of components with designed voids, adding material only where necessary. This allows for the creation of a lattice-like structure within the component, reducing mass, especially in areas near the axis of rotation, without significantly compromising bending strength.

Following, special attention is given to evaluating the flexural mechanical properties of MEX and MIM samples, considering the impact of the mass and geometric density of the specimens. The primary objective of this study is to determine the relationship between flexural resistance and component mass and how far printed samples diverge from injected.

2. MATERIALS AND METHODS

2.1 MATERIALS

Commercial Farlabor carbonyl iron powder was used in this work as a dispersed constituent in the MIM feedstock. This raw material was fabricated by mixing PP, EVA, paraffin, stearic acid, antioxidant and Fe carbonyl powder in an oil-heated laboratory-scale Sigma mixer. Afterward, it was processed as pellets in a Seibt industrial granulator to MIM process. Subsequently, the material that was not utilized in MIM, but derived from the same batch, was processed into powder using a 3-blade mill to be applied at the MEX machine. Then, the samples fabricated by MIM and MEX, designated as green samples, were submerged in hexane in a Lömi solvent debinding system to extract the soluble binders: paraffin and EVA. Now, the specimens demonstrate what is known as brown resistance. Specifically, it is the insoluble binder, the PP, that ensures the structural integrity and support for the specimens as a backbone. Finally, the brown samples were sintered using a plasma reactor, manufactured and patented, at Labmat (Florianópolis, SC). Subsequently, now with metallic Fe carbonyl samples (Fig. 1), bending tests were performed at a MTS universal test machine. The fractures of the samples were observed using scanning electron microscopy (SEM).

2.2 METHODOLOGY

The feedstock fabrication process, mixing was carried out using a Sigma mixer machine. The mixing procedure followed 1 hour at a temperature of 160 °C and a rotational speed of 70 rpm. To initiate the mixing, all the necessary materials were pre-mixed in a becker using a spoon. In a single operation, approximately 2 kg of feedstock was produced.

MIM process was conducted following pre-established parameters. The Arburg 320s machine was set with an injection pressure of 1000 bar and a mold closure force of 400 kN. The metal powder mixed with a binder was injected into the mold cavity at an injection speed of 160 mm/s and an injection temperature of 180 °C. The dosing stroke of 50 mm ensured control over the volume of material injected. Furthermore, the mold temperature was maintained at 50 °C to aid in the solidification and ejection of the molded parts.

MEX was conducted utilizing a 0.6 mm nozzle, heated to a temperature of 220 °C. The printing table was maintained heated till 100 °C to first layer printing and turned-off after that, ensuring specimens adhesion. Each layer of the specimen was deposited with layer thickness of 0,2 mm. The infill geometry of each specimen followed a grid pattern (Fig. 2).

Three samples of each infill volumes (25%, 50%, 75% and 90%) were fabricated. To maintain optimal printing speed and accuracy, the extrusion flow was set at 1 mm^3.s-1, allowing for consistent material flow and deposition.

During the chemical debinding, the soluble binders, paraffin and EVA, went through solubilization using a Lömi solvent debinding system. To dissolve the binders completely, they were submerged in an organic solvent (hexane) at 60 °C for a duration of 12 hours. In accordance with the experimental agenda, the debinding process was initially performed on the MIM samples, followed by the subsequent processing of the MEX samples.

For the plasma sintering process, gas flow rate was maintained at 500 SCCM (Standard Cubic Centimeters per Minute). The temperature profile consisted of three distinct steps. In the first step, of heating, the temperature increased from 0 to 300 °C at a rate of 5 °C.min-1, with a 100% H2 atmosphere. The power parameters employed were Ton = 100 µs (240 µs period) and applied voltage Tap = 400 V. Advancing to the second step, of thermal polymer extraction, the temperature was further elevated from 300 to 500 °C, at a rate of 1 °C.min-¹ maintaining a 100% H2 atmosphere, while maintaining the power settings of Ton = 100 V and Tap = 400 V. For to the third step, the temperature was raised from 500 to 1150 °C at a rate of 5 °C per minute, with the atmosphere adjusted to 5% H2 and 95% Ar. The power settings were adjusted to Ton = 50 µs and Tap = 400 V for this stage. At 1150 °C, the temperature was held steady for 1 hour. During this stage, the atmosphere and power settings was not changed. The last step, subsequent cooling process, the power parameters were further adjusted to Ton = 10 µs, and 100% H2 was employed as the atmosphere.

Flexural tests was conducted using the following parameters: a load cell with a capacity of 100 kN was employed to measure the applied load during the 3 points bending test. The distance between supports was set at 24,5 mm, ensuring proper specimen positioning. The test was conducted at a constant crosshead speed of 5 mm/min, allowing for a controlled and consistent rate of deformation during the flexural testing process according to ISO 178. The elastic module of the specimens were evaluated by the machine during the test and the elastic limit evaluated representing 0,02 mm of displacement in the force versus displacement graphic. Number of Samples tested 3 MEX samples of each infill volume and 6 MIM samples. Graphics was plotted with average results.

Finally, scanning electron microscopy (SEM) was applied to take some images from the fracture area of few samples.

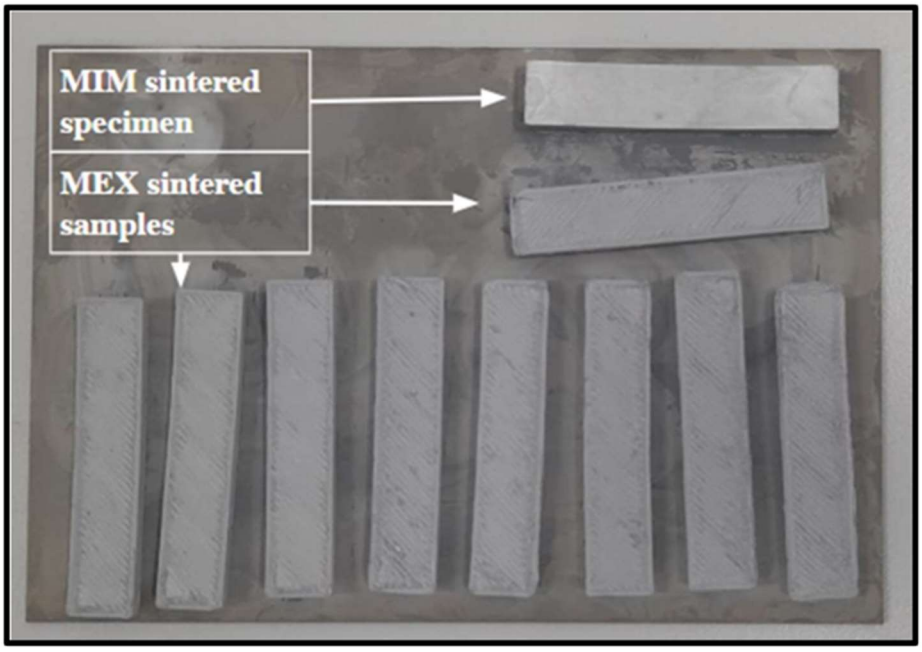

Figure 1. samples fabricated in this study by the authors.

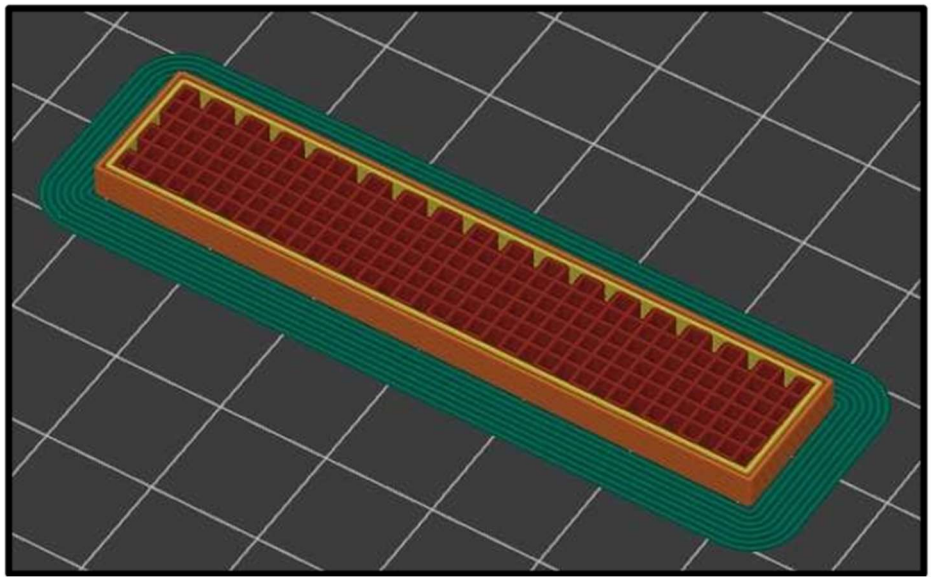

Figure 2. grid infill pattern is in red, while the walls are represented by orange and yellow. Additionally, the brim is indicated by green.

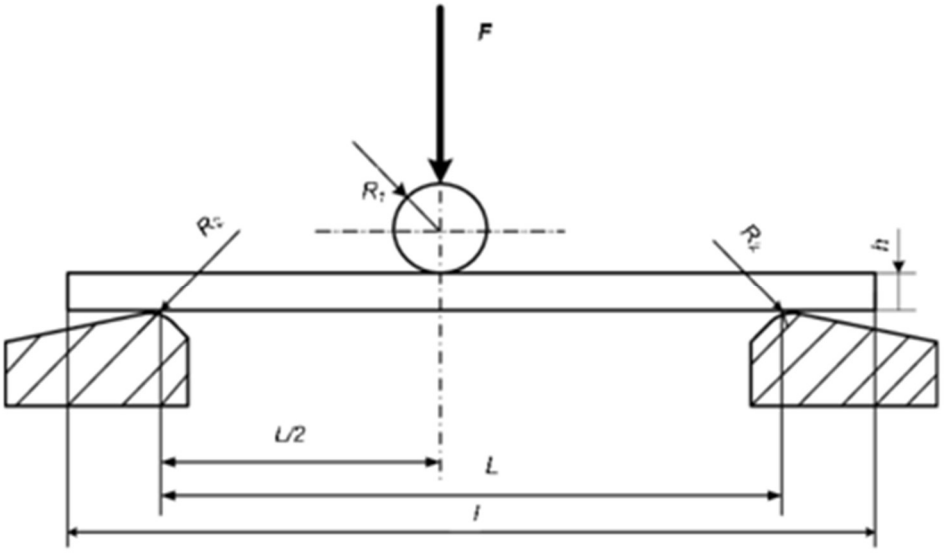

Figure 3. test setup according to ISO 178.

Figure 4. MTS universal test machine utilized in this study.

By measuring the applied force and knowing other geometric parameters, such as the distance between supports and the dimensions of the test specimen, which in this case is a rectangular parallelepiped, it is possible to derive additional information. This is because the moment of inertia of the area is determined based on the cross-sectional profiles, especially for simple geometries, as is the case with test specimens, which are rectangular in shape. For a rectangular section profile, the moment of inertia is defined as presented in Eq. (1):

$$I = (b * h^3) / 12 \quad (1)$$

Where:
I - Moment of inertia of the área
b - Width of the rectangle with respect to the axis of rotation
h - Height of the rectangle with respect to the axis of rotation

It's worth noting that, in the case of a rectangle, the height contributes significantly more than the width to the moment of inertia. Which as previous pointed out that this is one of the highlights of MEX.

Also is possible to determine the maximum bending moment in a simply supported beam using the formula in Eq. (2):

$$M = (P * L^2) / 8 \quad (2)$$

Where:
M - Maximum Bending Moment
P - Applied Load (measured during testing)
L - Distance between supports (25.4 mm)

With this information, you can calculate the stress at the maximum distance to the neutral axis using Eq. (3):

$$\sigma = M * c / I \quad (3)$$

Where:
σ - Stress at maximum distance to the neutral axis (maximum stress)
c – maximum distance to the neutral axis

However, the results will be presented as load versus displacement curves for various test specimens. The internal lattice geometry leads to differing moments of inertia depending on the sample's length, whether the infill is transverse or longitudinal. As a result, although it is possible to calculate the stress, it might not accurately reflect real-world conditions, since that in ideal samples and with all the precise information, the stresses should be the same for all samples, as it is the same material. So, a direct comparison of the forces versus displacement by various test specimens under uniform testing conditions was the preferred approach.

Furthermore, tension tests have been previously conducted in accordance with the standard test for stress, using a similar comparative methodology for injected and MEX-fabricated samples (Vidal et al., 2022)

3. RESULTS AND DISCUSSIONS

The results of the bending tests, in terms of force (kN) versus displacement (mm), are presented in Figure 5. As expected, the MIM samples displayed higher resistance in terms of elastic limit and ultimate force before relatively large amounts of strain localize disproportionately in a small region of the specimen (necking). The first notable result pertains to the 75% and 90% infill MEX samples, which exhibited behavior most similar to that of the MIM sample, particularly in terms of elastic limit and ultimate force-to-density ratio. The 90% and 75% MEX samples were almost overlapping, even though the ultimate strength of the 75% MEX sample was slightly higher. The expected outcome was for the 90% sample to exhibit higher ultimate force, but this was not the case. One hypothesis is that printing failures, as illustrated at figure 6, adversely affected the properties of this specific sample. Consistent with expectations, the 25% infill sample performed the poorest in terms of elastic limit and ultimate force.

Mechanical properties evaluated are presented in Table 1. The elastic limit of the 75% infill MEX samples was around 16% lower than that of the MIM samples. This is remarkable, considering that the 75% infill samples have approximately 14% less mass compared to the MIM-fabricated samples. In the same way, 90% infill samples reached an elastic limit 15% lower and a decreasing of 9% the component mass. Furthermore, the infill geometry can be optimized, and printing defects can be resolved in further studies to improve these results. On a larger scale, saving approximately 9 or 16% of raw material can have a game-changing impact in terms of conserving natural resources.

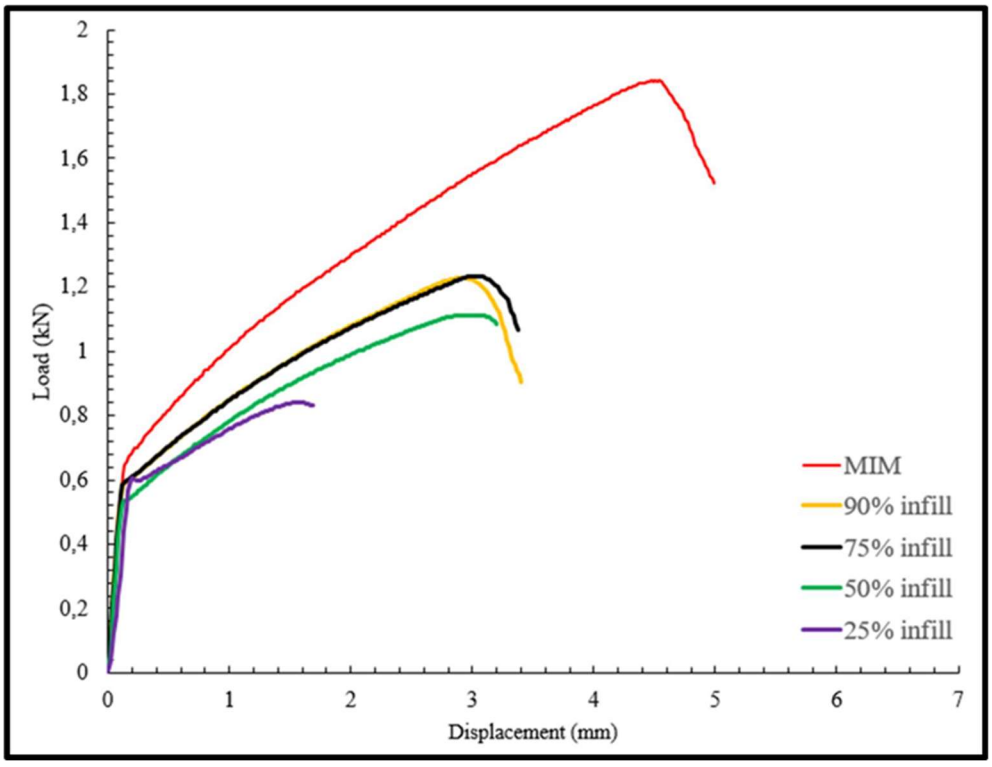

Figure 5. bending tests results.

As presented in figure 5, initially, the force required for deformation up to the elastic limit closely mirrors that MIM counterparts. This resemblance arises from the fact that, during elastic behavior, porosity within these materials does not serve as a stress concentrator. Nevertheless, a critical shift occurs beyond the elastic limit. Here, the pores and defects caused by additive manufacturing (figure 6) within the MEX samples begin to function as stress concentrators, channeling the applied stress and accelerating the accumulation of dislocations. Consequently, the material experiences premature failure.

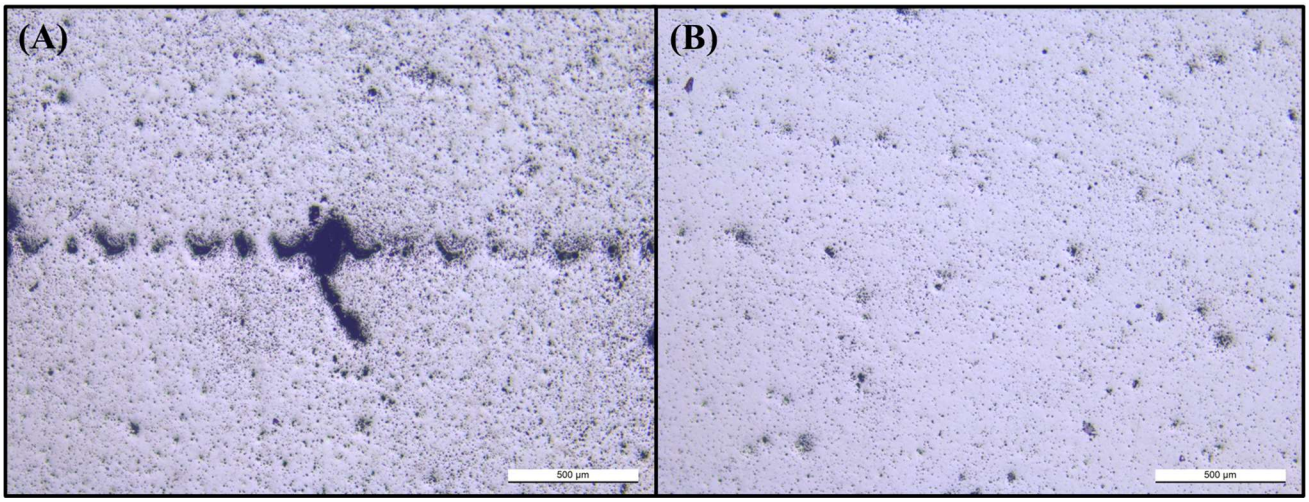

Figure 6. (A) an example of a line printing defect caused by adhesion problems between two consecutives printed layers. Furthermore, porosity from sintering process is visible. (B) MIM sample illustrating pores from sintering.

Table 1. mechanical properties evaluated from bending tests.

Composite Properties	**MIM**	**25% Infill**	**50% Infill**	**75% Infill**	**90% Infill**
Mass, g	14,5444 ± 0,01	10,6207 ± 0,30	12,1406 ± 0,20	13,2944 ± 0,47	13,6183 ± 0,07
Density, g/cm³	6,3819 ± 0,22	4,6793 ± 0,25	5,0954 ± 0,26	5,411 ± 0,31	5,5211 ± 0,20
Elastic limit, N	920	720	717	772	779
Ultimate force, N	1842	841	1112	1234	1229
Ultimate Force-to-Density ratio, N.cm³/g	289	180	218	228	223

3.1 SCANNING ELECTRON MICROSCOPY (SEM)

At the fracture region, SEM images were taken for a qualitative comparison between a sample of MIM and the MEX sample with 25% infill. The images in Figure 7 reveal a significant amount of porosity in the bulk material region, likely originating from the sintering process. One hypothesis to explain this observation is the coarse granulometry of the Fe carbonyl powder (~15 µm). It is expected that reducing the powder's particle size would result in less porosity. On the other hand, it appears that the porosity volume is relatively similar in the bulk regions of the compared samples.

In Figure 8, the explicit presence of cavities and the internal geometry of the MEX sample can be observed. The overall appearance of the bulk material remains similar. However, a printing line defect is visible in the MEX sample. By optimizing the fabrication of the feedstock, refining the MEX process parameters, and improving the sintering conditions, it is possible to achieve a superior microstructure characterized by reduced porosity volume and enhanced structural integrity.

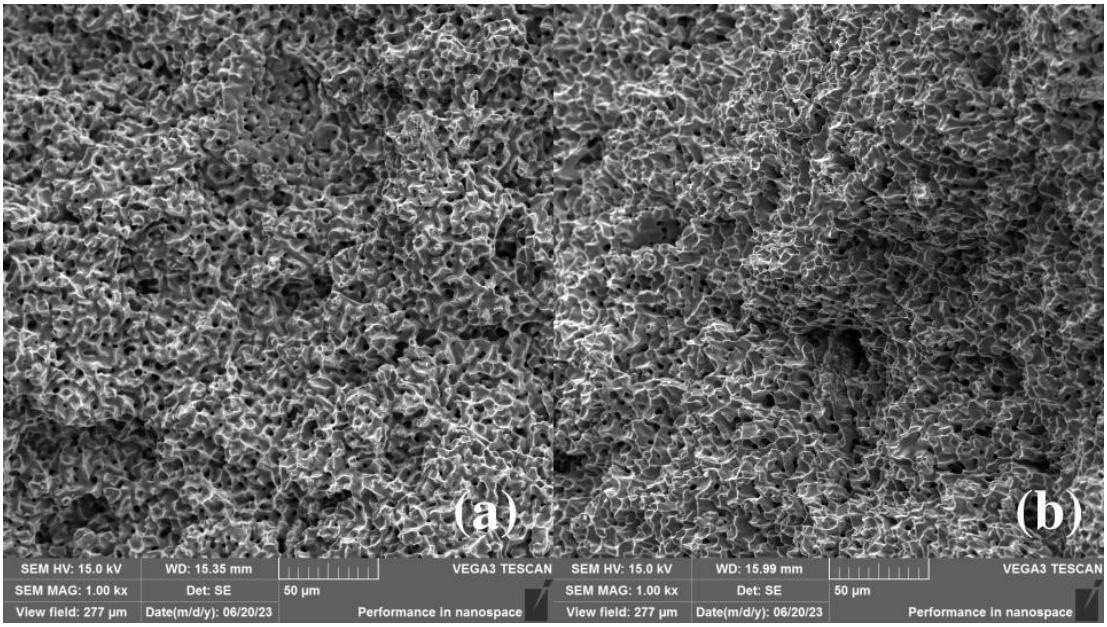

Figure 7. (a) MIM sample. (b) MEX 25% infill sample.

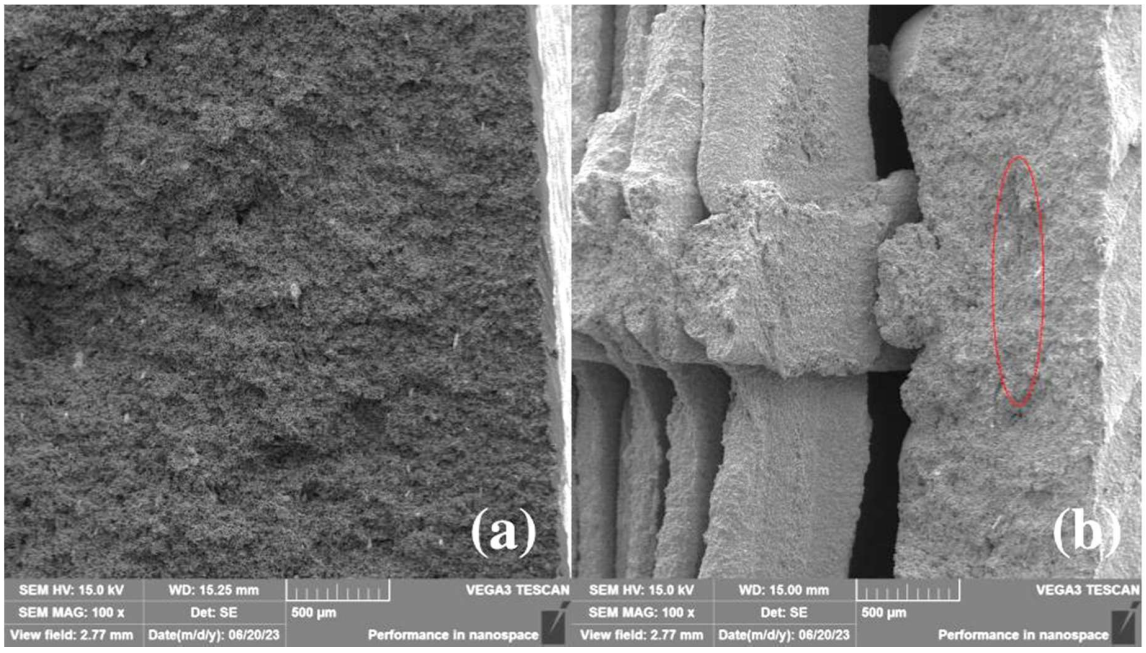

Figure 8. (a) MIM sample. (b) MEX 25% infill sample. Within the red line in image (b), a line defect resulting from the printing process is visible.

4. CONCLUSIONS

The following topics present the conclusions from this study:

1. It was possible to produce and test metallic flexural test samples with internal cavities that are not connected to the specimen's surface through material extrusion additive manufacturing. No other traditional manufacturing method can achieve this characteristic.
2. The MEX samples with 75% and 90% infill volume achieved better properties among MEX samples when compared to MIM samples in terms of elastic limit and ultimate force. Additionally, these samples had 16% and 9% less mass than injected specimens, respectively. These results demonstrate that applicable properties can be

attained for products manufactured through AM while significantly reducing the amount of raw material used in the process.

3. The 75% infill specimens among the MEX samples achieved the highest ultimate strength-to-density ratio. These results further support the concept of achieving structurally applicable properties through AM, such as MEX, while simultaneously reducing the consumption of natural resources as raw material.

The primary objective of this study, which was to determine the relationship between flexural resistance and component mass, has been achieved. The optimization of printing parameters, mitigation of fabrication defects, and exploration of alternative infill geometries specifically designed for various applications are expected to further enhance the properties of MEX products.

5. REFERENCES

Astakhov, V.P., 2010. *Geometry of Single-point Turning Tools and Drills*. Springer, Londres.

Beeley, P., 2001. *Foundry Technology, 2nd Edition*. Butterworth Heinemann, Oxford

Gibson, I., Rosen, D., and Stucker, B., 2010. *Additive Manufacturing Technologies: 3D Printing, Rapid Prototyping, and Direct Digital Manufacturing*, *2nd edition*. Springer, New York.

Gonzalez-Gutierrez, J., Cano, S., Ecker, J. V., Kitzmantel, M., Arbeiter, F., Kukla, C., and Holzer, C, 2021. *Bending properties of lightweight copper specimens with different infill patterns produced by material extrusion additive manufacturing, solvent debinding and sintering*, Applied Sciences.

Suwanpreecha, C., Songkuea, S., Linjee, S., Muengto, S., Bumrungpon, M., and Manonukul, A., 2023. *Tensile and axial fatigue properties of AISI 316 L stainless steel fabricated by materials extrusion additive manufacturing*. Materials Today Communications, 35.

Vidal, A.A., Zanetti, F.I., Lau, G.A., Klein, A.N., and Cardoso, R.P., 2022. “Injection Molding feedstock applied to Additive Manufacturing: First results and evaluation by tensile strength tests”. In Proceedings of the 20nd Brazilian Materials Research Society Meeting - B - MRS 2020. Foz do Iguassú, Brazil.

6. RESPONSIBILITY NOTICE

The authors are the only responsible for the printed material included in this paper